- Technical Paper -

THREE-DIMENSIONAL MESOSCOPIC SIMULATION OF CONCRETE UNDER BIAXIAL STRESS CONDITION BY RBSM

Kohei NAGAI[*1], Yasuhiko SATO[*2] and Tamon UEDA[*3]

ABSTRACT

Concrete is a heterogeneity material consisting of mortar and aggregate at meso scale. Evaluation of fracture process in this scale is useful to clarify the material characteristics of concrete. The authors have conducted meso scale analysis of concrete over a past few years by Rigid Body Spring Model (RBSM). In this study, three-dimensional RBSM analysis of concrete under biaxial compression stress condition is carried out where the analysis simulates the crack in normal direction to plane of specimen, which cannot be presented by two-dimensional RBSM analysis.

Keywords: 3D RBSM, meso scale analysis, biaxial compression stress condition, Voronoi geometry

1. INTRODUCTION

Concrete is a heterogeneous material consisting of mortar and aggregate at meso level. Evaluation of the fracture process at this level is useful to clarify the material characteristic of concrete. However, the analytical approach at this level has not yet been sufficiently investigated. The Authors have conducted the two- and three-dimensional mesoscopic analysis of failure of concrete by Rigid Body Spring Model (RBSM) over the past few years [1][2]. This analysis method is useful to simulate a discrete behavior like concrete fracture. On 3D RBSM, Toi et al. have carried out the research on damage mechanics model for brittle micro cracking solids [3]. Simulation of concrete or concrete structure by 3D RBSM is conducted in late years [4][5].

In the 2D RBSM by the authors [1], it has been confirmed that the analysis cannot simulate the biaxial compression failure because cracks in normal direction to the plane of the specimen, which is the primary cause of failure under biaxial compression, cannot be represented. This behavior can be simulated by only three-dimensional analysis. In this study, analysis of biaxial compression test of concrete is carried out by 3D RBSM. The difference of crack pattern under uniaxial and biaxial compression stress is discussed with comparing with two-dimensional RBSM analysis.

2. METHOD OF ANALYSIS

The RBSM developed by Kawai is one of discrete numerical analysis method [6]. The analytical model is divided into polyhedron elements whose phases are interconnected by springs. Each element has three transitional and three rotational degrees of freedom at some point inside of the element. One normal and two shear springs are placed at the centroid of each face (Fig.1). Since cracks initiate and propagate along the boundary face, the element arrangement may affect fracture direction. To avoid formation of cracks in a certain direction, small element size, which is 2.5~3.0mm^3, and a random geometry are introduced using a three-dimensional Voronoi diagram. The Voronoi diagram is the collection of Voronoi cells (Fig.2). Each cell represents mortar or aggregate element in the analysis.

In the nonlinear analysis, stiffness matrix is constructed by the principle of virtual work [6], and the Modified Newton-Raphson method is employed for the convergence algorithm. When the model does not converge at the given maximum iterative calculation number, analysis proceeds to the next step.

3. MATERIAL MODELS FOR 3D RBSM

3.1 Mortar Model

In this study, a constitutive model for mortar

*1 JSPS Post-doctoral fellow, Swiss Federal Institute of Technology Zurich, Dr.E., JCI Member
*2 Associate Professor, Hokkaido University, Dr.E., JCI Member
*3 Professor, Hokkaido University, Dr.E., JCI Member

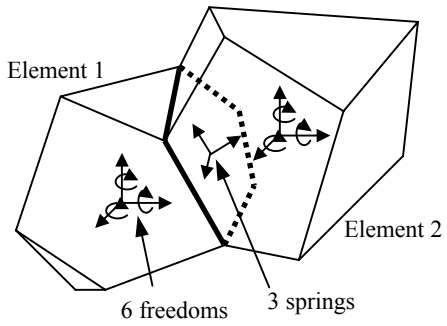

Fig. 1 Mechanical model

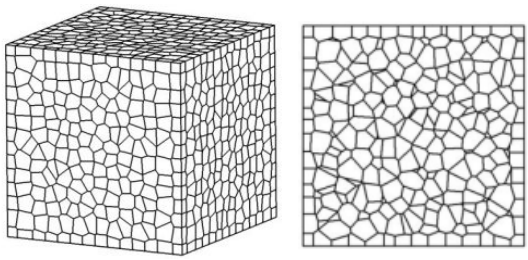

a) 3D view b) Cross section

Fig. 2 3D Voronoi geometry

at meso level is developed because the constitutive model in macro scale cannot be applied to meso scale analysis.

The material characteristics of each component are presented by means of modeling springs. In normal springs, compressive and tensile stresses (σ) are developed. Shear springs develop shear stress (τ). The elastic modulus of normal spring (k_n) and shear spring (k_s) are presented as follows,

$$k_n = \frac{(1-\nu_{elem})E_{elem}}{(1-2\nu_{elem})(1+\nu_{elem})} \qquad (1)$$
$$k_s = \frac{E_{elem}}{1+\nu_{elem}}$$

where k_n and k_s are the elastic modulus of normal and shear spring, E_{elem} and ν_{elem} are the elastic modulus and Poisson's ratio of component for meso level, respectively.

In the analysis, due to the original characteristics of RBSM, the values of the material properties at the meso level given to the elements are different from the material properties of the object analyzed at the macroscopic level. In this study, the material properties for the elements were determined in such a way as to give the correct macroscopic properties. For this purpose, the elastic analysis of mortar in compression was carried out. In the elastic analyses, the relationship between the macroscopic and mesoscopic Poisson's ratios and the effect of the mesoscopic Poisson's ratio on the macroscopic elastic modulus were examined. From the results (Fig. 3), Eqs. (2) and (3) are adopted for determining the mesoscopic material properties.

$$\nu_{elem} = -24.8\nu^4 + 31.9\nu^3 - 16.4\nu^2 + 4.28\nu \qquad (0 \leqq \nu \leqq 0.3) \qquad \cdots\cdots (2)$$

$$E_{elem} = (-33.7{\nu_{elem}}^4 + 17.0{\nu_{elem}}^3 - 4.13{\nu_{elem}}^2 + 0.327\nu_{elem} + 1)E \qquad \cdots\cdots (3)$$

where E and ν are the macroscopic elastic modulus and Poisson's ratio of component of the analyzed object, respectively.

Only the maximum tensile stress has to be set as a material strength. Actually, mortar itself is not a homogeneous material, which is consisting of sand and paste, even when bleeding effect is ignored. Strength variation in mortar has not been clarified yet. In this study, a normal distribution is assumed for the tensile strength of spring element. The probability density function is as follows [1],

$$f(ft_{elem}) = \frac{1}{\sqrt{2\pi}\sigma}\exp\left\{-\frac{(ft_{elem}-\mu)^2}{2\sigma^2}\right\} \qquad (4)$$
$$\mu = ft_{average}$$
$$\sigma = -0.2\,ft_{average} + 1.5$$

when $f_{t\,elem} < 0$ then,

$$f_{t\,elem} = 0$$

where $f_{t\,elem}$ is the distributed tensile strength and $f_{t\,average}$ is the average tensile strength of mortar at the meso level. The same distribution is given to the elastic modulus. Those distributions affect the macroscopic elastic modulus, so that the elastic modulus for the element given by Eq.(2) is multiplied by 1.05.

Springs set on the face behave elastically until stresses reach the τ_{max} criterion or tensile strength. The strains and stresses are calculated as follows.

$$\varepsilon = \frac{\delta_n}{h_1 + h_2} \qquad (5)$$
$$\gamma = \frac{\delta_s}{h_1 + h_2}$$
$$\sigma = k_n\varepsilon$$
$$\tau = k_s\gamma$$

where ε and γ are the strain of normal and shear springs, respectively. δ_n and δ_s are the normal and shear relative displacement of elements of those springs, respectively. h is the length of

perpendicular line from the calculation point of element to the boundary face. Subscripts 1 and 2 represent elements 1 and 2 in Fig.1, respectively.

Constitutive model of normal spring is shown in Fig. 4. In compression zone, it always acts elastic. Fracture happens between elements when spring reaches tensile strength $f_{t\,elem}$, and the normal stress decreases linearly depending on crack width that is the spring elongation. In this study, stress-free crack width w_{max} is set 0.03mm. The linear unloading and reloading path that goes through the origin is introduced to normal spring in tension zone. For shear spring, elasto plastic model is applied as shown in Fig.5 in the range that normal spring dose not have fracture. And the linear unloading and reloading path is introduced. Value of τ_{max} changes depending on the condition of normal spring and given as follows,

$$\tau_{\max} = \pm(0.30 f_{telem}{}^{2.5}(-\sigma + f_{telem})^{0.4} + 0.15 f_{telem}) \quad (\sigma < f_{telem}) \quad \cdots\cdots (6)$$

When fracture happens in normal spring, the calculated shear stress is reduced corresponding to the reduction ratio of normal stress. As a result, shear spring cannot carry the stress when crack width of normal spring reaches w_{max}.

In this study, normal springs in compression only behave elastically and never break nor have softening behavior.

3.2 Aggregate Model

In this study, element of aggregate behaves only elastic without fracture. The same equations as Eqs.(1), (2), (3) and (5) are adopted to present the material property of aggregate.

3.3 Interface Model

The same stress-strain relationships as Eq.(5) and strength and stiffness distribution as Eq.(4) are adopted for the material properties of the interface between mortar and aggregate. The spring stiffnesses k_n and k_s (Eq.(1)) of the interface are given by a weighted average of the material properties in two elements according to their length of perpendicular line from the calculation point of element to the boundary face where springs are set.

Similar constitutive models of the spring between mortars are applied to the interface springs. For the normal spring, the constitutive model in Fig. 4 is adopted. For the interface spring, w_{max} is set 0.0025mm. For shear springs, an elasto plastic model as shown in Fig. 5 is applied. The τ_{max} criterion for the interface as shown in Eq. (7) and Fig. 6 is adopted.

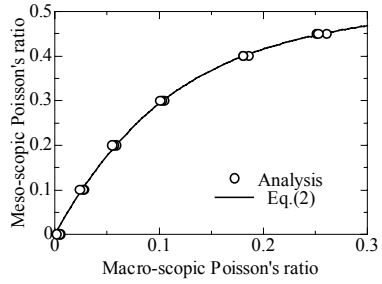

a) Poisson's ratio

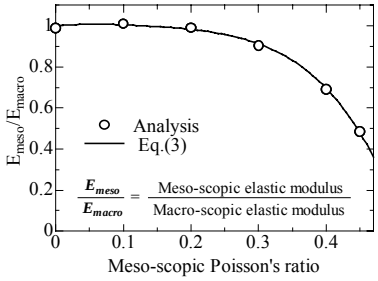

b) Elastic modulus

Fig. 3 Effect of mesoscopic material properties on macroscopic properties

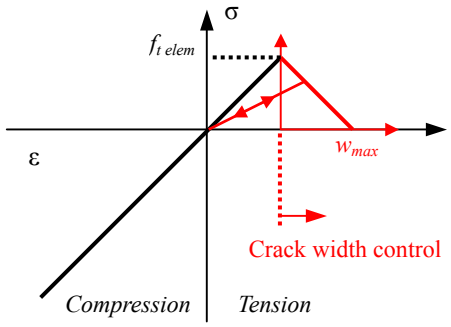

Fig. 4 Model of normal spring

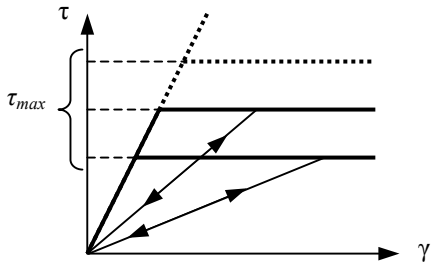

Fig. 5 Model of shear spring

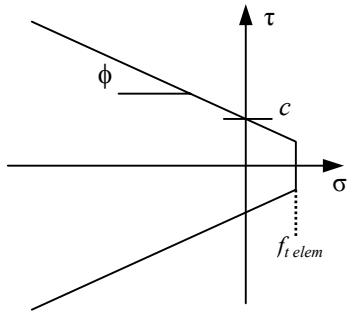

Fig. 6 τ_{max} criterion for interface

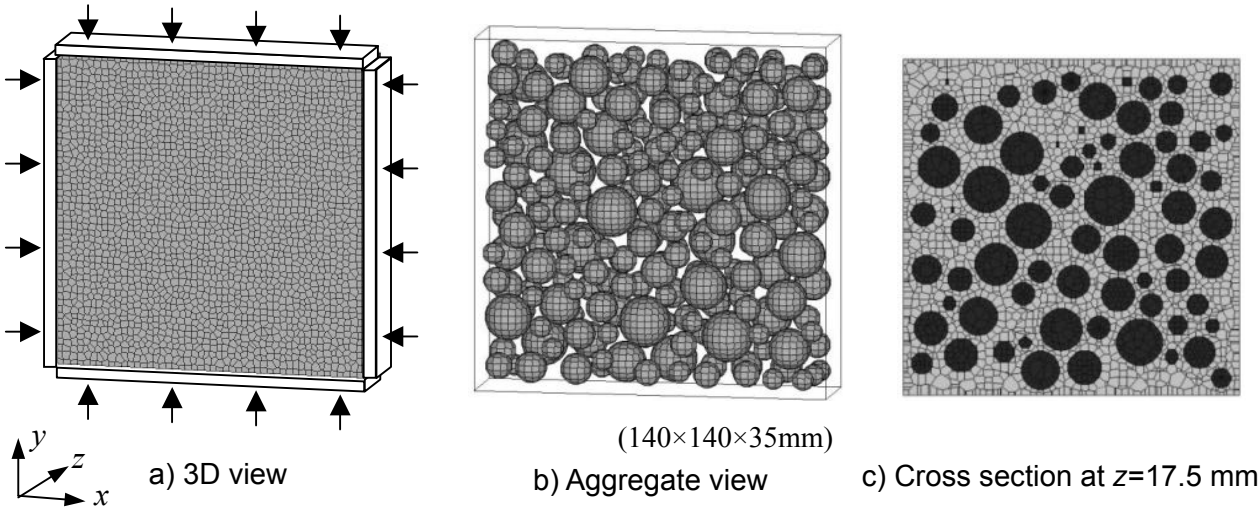

a) 3D view b) Aggregate view c) Cross section at z=17.5 mm

Fig. 7 Analyzed specimen

Table 1 Material property

Mortar		Aggregate		Interface	
$f_{t\,average}$	3.48 MPa	-	-	$f_{t\,average}$	1.63 MPa
Elastic modulus (E)	21,876 MPa	Elastic modulus (E)	50,000 MPa	c	2.69 MPa
Poisson's Ratio (v)	0.18	Poisson's Ratio (v)	0.25	ϕ	35°

$$\tau_{\max} = \pm(-\sigma \tan\phi + c) \qquad (\sigma < f_{telem}) \tag{7}$$

where ϕ and c are constant values. This criterion is based on the failure criterion suggested by Taylor and Broms [7] and Kosaka et al. [8], which is derived from experimental results. Similarly to the spring between mortars, when fracture happens in normal spring, the calculated shear stress is reduced according to the reduction ratio of normal stress.

4. ANALYSIS

4.1 Specimen for Analysis

Figure 7 shows the analyzed specimen, aggregates inside of the specimen and cross section at z=17.5 mm. Size of the specimen is 140×140×35 mm and the number of element is 34,535. The aspect ratio of the specimen is same as the experiment by Kupfer et al. [9] though the size is smaller due to the high cost of calculation time. The average element size is 2.71 mm^3. Shape of aggregate is sphere in this study. The Voronoi diagram on the surface of the aggregate is controlled for the configuration of the sphere shape. Size and number of the aggregate are decided based on the JSCE Standard Specification for Concrete Structures [10] and the maximum aggregate size is set 20 mm. However, due to the difficulty of forming sphere shape with the small size, the aggregates whose diameters are not more than 6 mm are eliminated. Hence the aggregate volume in the specimen becomes lower than that in usual concrete. The aggregate ratio in the specimen is 27.9%. Input material properties are determined by the flowchart developed by the authors [1] in which the values are calculated from the target compressive strength of mortar. The target compressive strength of mortar is set 35 MPa. The calculated material properties are indicated in Table 1.

Biaxial compressive loading is applied (see Fig. 7 a)). Displacement is controlled in the analysis and the applied displacement ratio in two axes is -1:-1. The friction between the specimen and the loading boundary is eliminated. Uniaxial compression test of the specimen is also carried out where the side boundaries are not set.

For the comparison with three-dimensional analysis, 2D RBSM analysis of similar specimen is conducted with the analysis system developed by the authors [1]. The size of the specimen is 140×140 mm and the number of element is 2,917 (Fig. 8). Material properties and the loading condition are same as those in three-dimensional analysis.

4.2 Result of Analysis

Stress strain curves in Fig. 9 show the predicted results of analyses. In uniaxial tests, although strength in two-dimensional analysis is lower than that in three-dimension, similar curves are simulated. The uniaxial compressive strength in three-dimensional analysis is 29.36 MPa. Figures 10 and 11 show the deformation of 2D and

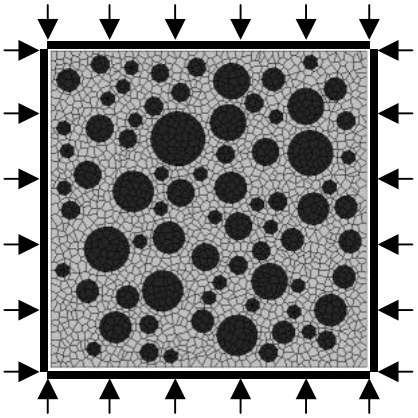

Fig. 8 2D RBSM specimen

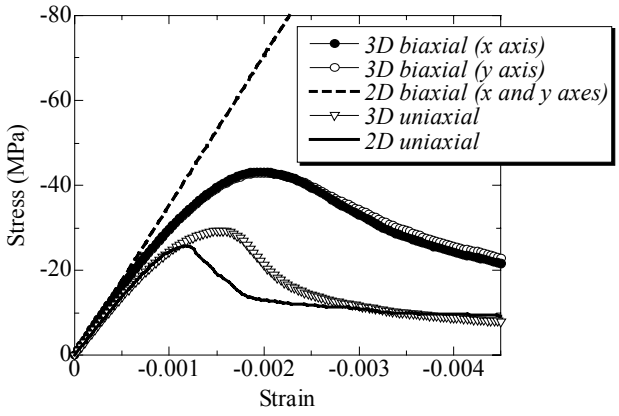

Fig. 9 Stress strain relationships

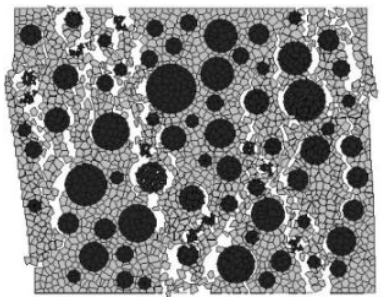

Deformation × 5

Fig. 10 Failure view
(2D uniaxial test)

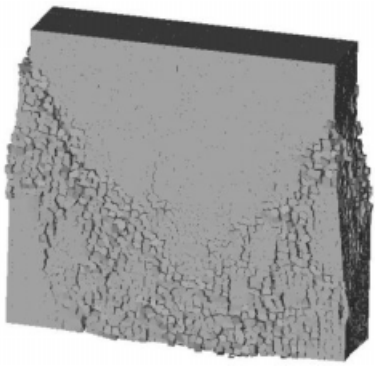

Deformation × 5

Fig. 11 Failure view
(3D uniaxial test)

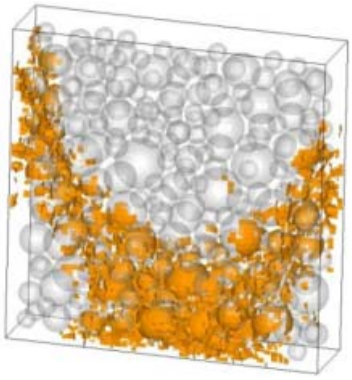

0.3 mm

Fig. 12 Internal crack at failure
(3D uniaxial test)

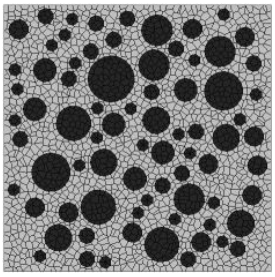

Deformation × 5

Fig. 13 Deformation at
stress of 80 MPa
(2D biaxial test)

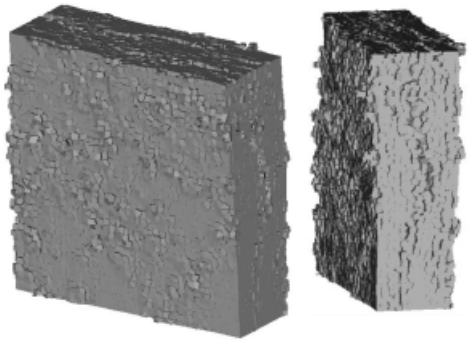

a) Whole view b) From side

Deformation × 5

Fig. 14 Failure view
(3D biaxial test)

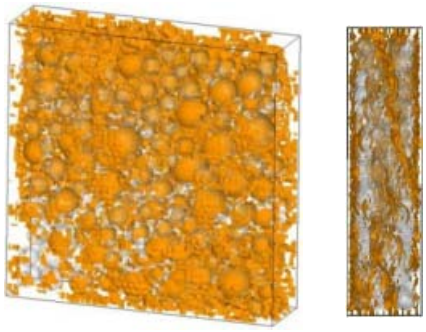

a) Whole view b) From side

0.3 mm

Fig. 15 Internal crack at failure
(3D biaxial test)

3D specimens at strain of –4,500μ. The transitional deformation is enlarged 5 times. And the internal faces reaching 0.3 mm crack width at the same strain in 3D specimen is presented in Fig.12. Similar major crack patterns forming approximately 20~30 degrees with respect to the loading axis are simulated.

In biaxial test, only three-dimensional analysis predicts the reduction of stress where the strength in *y*-axis is 42.91 MPa. The ratio of strength in biaxial test (-1:-1) to that in uniaxial strength is 1.46. In the failure criterion model suggested by Kupfer [9], the ratio under -1:-1 loading ratio is 1.16 therefore the analysis overestimates the strength under biaxial compression stress condition. In two-dimensional analysis, the specimen behaves almost elastic. The deformation of 2D specimen at stress of 80 MPa is

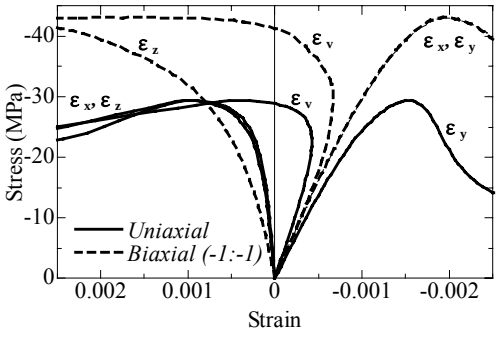

Fig. 16 Stress strain curves in 3D analyses

shown in Fig. 13 where no fracture is observed because the analysis cannot simulate the crack in normal direction to the plane of the specimen. In contrast, the normal crack to the plane of the specimen is simulated in three-dimensional analysis as shown in Figs. 14 and 15 where the deformation at strain of –4,500μ and the internal crack faces reaching 0.3mm are presented. This crack pattern is different from that in uniaxial test (see Fig. 11), which is same behavior as observed in the experiment [9].

Figure 16 shows the stress-strain and stress-volumetric strain relationships in three-dimensional analyses. The strains are calculated using the relative deformations of the elements on the surface of specimen. In uniaxial analysis, the specimen comes to failure just after the volumetric strain change becomes increase from decrease. On the other hand, the stress increases by more than 10 MPa after the volumetric strain start to increase in biaxial analysis. In the experiment, specimen fails just after the volumetric strain starts to increase in both cases [9]. This difference might be improved if the fracture in normal direction to the plane of the specimen can propagate smoothly around the peak stress under the biaxial compression stress condition in the analysis.

5. CONCLUSIONS

(1) Both 2D and 3D RBSM analyses simulate similar failure pattern of concrete under uniaxial compression stress condition.
(2) In 2D RBSM analysis, specimen dose not show the reduction of stiffness and behaves elastically under biaxial compression stress condition.
(3) The crack in normal direction to the plane of specimen under biaxial compression stress condition, which is primary cause of the failure, is simulated reasonably by 3D RBSM analysis.
(4) In the 3D analysis, the ratio of strength under biaxial compression to that in uniaxial compression is overestimated. The development of lateral strain in the direction normal to the biaxial compression plane is not well simulated.

REFERENCES

[1] K. Nagai, Y. Sato and T. Ueda: Mesoscopic Simulation of Failure of Mortar and Concrete by 2D RBSM, Journal of Advanced Concrete Technology, JCI, Vol. 2, No. 3, pp.359-374, 2004
[2] K. Nagai, Y. Sato and T. Ueda: Three-dimensional Meso-scopic Analyses of Mortar and Concrete Model by Rigid Body Spring Model, Proceeding of FRAMCOS-5, Vol. 1, pp.353-360, 2004
[3] Y. Toi and T Kiyosue: Damage Mechanics Model for Brittle Microcracking Solids Based on Three-dimensional Mesoscopic Simulation, Engineering Fracture Mechanics, Vol.50, No.1, pp.11-27,1995
[4] J.E. Bolander and S. Berton: Cohesive Zone Modeling of Fracture in Irregular Lattices, Proceedings of FraMCos-5, Vol.2, pp.989-994, 2004
[5] T. Suzuki, S. Saito and I. Higai: Fracture Analysis of RC Member using a 3-D Rigid-Body-Spring Model, Proceedings of JSCE annual conference 2004, pp.755-756, 2004 (in Japanese)
[6] T. Kawai and N. Takeuchi: Discrete Limit Analysis Program, Series of Limit Analysis by Computer 2, Bifukan, Tokyo, 1990 (in Japanese)
[7] M.A. Taylor, and B.B. Broms; Shear Bond Strength Between Coarse Aggregate and Cement Paste or Mortar, Journal of the ACI, Vol.61, No.8, pp.939-956, 1964
[8] Y. Kosaka, Y. Tanigawa and M. Kawakami: Effect of Coarse Aggregate on Fracture of Concrete (part 1), Journal of AIJ, Vol.228, pp.1-11, 1975 (in Japanese)
[9] Kupfer, H., Hilsdorf, H., K. and Rusch, H.: Behavior of Concrete under Biaxial Stresses, ACI Journal, Vol.66, No.8, pp.656-666, 1969
[10] JSCE: Standard specification for concrete structures, Materials and construction, JSCE, 2002 (in Japanese)